Review

Pharmaceutical BIOPROCESSING

Pharm. Bioprocess.
(2014) 2(1), 85–99

Computational fluid dynamics as a modern tool for engineering characterization of bioreactors

Since design, construction and evaluation of bioreactors for large-scale production is costly and time consuming, computational methods may give some insights into the fluid mechanics within bioreactors. Thus, critical limiting factors, such as insufficient mixing as well as inhomogeneous nutrient and oxygen mass transfer, may be identified early in the design process. Although advanced experimental techniques such as laser Doppler anemometry and particle image velocimetry are also reliable, they are too time consuming to characterize the complete flow pattern in industrial scales and rely on optical accessibility. Therefore, the knowledge of flow characteristics provided by computational fluid dynamics (CFD) is indispensable for the rational design of bioreactors. Based on previously published reviews, the present work summarizes the latest publications on the usage of CFD to characterize and scale-up bioreactors used in biotechnological processes. Selected models that are used to predict the fluid flow pattern and key engineering parameters of commonly used bioreactors are described. Related issues, such as grid dependency of CFD results and the requirement for experimental verification are also addressed. Finally, an overview of proposed but not yet feasible CFD applications is presented, including fluid–structure interaction, the use of direct numerical simulation and the coupling fluid flow and chemical reactions.

Sören Werner*[1], Stephan C Kaiser[1], Matthias Kraume[2] & Dieter Eibl[1]

[1]Zurich University of Applied Sciences, School of Life Sciences & Facility Management, Institute of Biotechnology, CH-8820 Wädenswil, Switzerland

[2]Technische Universität Berlin, Chair of Chemical & Process Engineering, D-10623 Berlin, Germany

*Author for correspondence:
Tel.: +41 58 934 50 00
Fax: +41 58 934 50 01
E-mail: soeren.werner@zhaw.ch

It is essential that the characterization and optimization of fluid flows in bioreactors is performed, due to the sensitivity of the biological entities to environmental changes. The animal and plant cells that are often used for the production of modern pharmaceutical and cosmetic compounds are particularly sensitive to chemical and physical stresses [1,2]. The occurrence of chemical stress can often be ascribed to inhomogeneities, which can be prevented by better mixing performance, established by increasing the power input. In the case of shear sensitive cells, a compromise has to be found between the power input necessary to generate sufficient mass transfer and the risk of excessive power input generating critical shear stress levels. Thus, the bioreactors and the fluid flow inside the vessel should be well characterized. If the main engineering parameters, such as power input, mixing time and (oxygen) mass transfer coefficient, are known, it is possible to optimize cell growth and productivity, while maintaining high product quality. Furthermore, time- and cost-intensive trial-and-error experiments can be reduced, which is especially important if the availability of the biological material is limited, as is the case for primary tissues or stem cells.

When considering the heterogeneous distribution of shear stress and turbulence within most bioreactors, the need for spatially resolved flow data becomes clear [3]. These data can be gathered by experimental methods and/or simulations using computational methods. Computational fluid

FUTURE SCIENCE

10.4155/PBP.13.60 ISSN 2048-9145

Table 1. Glossary of symbols used throughout this article.

Symbol	Description	Symbol	Description
Latin symbols			
a	Specific surface	S	Source term (in momentum balance)
A_G	Surface of gas bubbles	S_k	Source term (in multi-phase momentum balance)
B_b	Birth of bubble due to break-up	t	Time
B_c	Birth of bubble due to coalescence	t_m	Mixing time
C_1	Constant (for oxygen diffusitivity)	$\overline{\overline{T}}$	Stress tensor (second rank)
$C_{1\varepsilon}$, $C_{2\varepsilon}$, C_μ, $C_{1\varepsilon}$	Empirical constants for turbulence models	$\vec{u}$	velocity vector
d_B	Diameter of gas bubbles	$\tilde{u}_i$	rotated velocity vector
D_b	Death of bubble due to break-up	$\bar{u}$	Time-averaged velocity
D_c	Death of bubble due to coalescence	u´	Fluctuation velocity
D_L	Oxygen diffusivity	V	Volume
dO_2	Solved oxygen concentration	X	Biomass concentration
dO_2^*	Maximal solved oxygen concentration	x,y,z	3D Cartesian coordinates in Euklidean space
d	Diameter of stirrer	$\tilde{x}$, $\tilde{y}$, $\tilde{z}$	3D Cartesian coordinates in Euklidean space, rotated to main flow direction
D_T	Local eddy diffusivity	*Greek symbols*	
f	Bubble number density	α, α_G	Phase fraction, of gaseous phase
$\vec{g}$	Gravitational acceleration	ε, ε_L	Turbulent energy dissipation rate, in liquid phase per unit mass
G_k	Term for the generation of turbulent kinetic energy	μ, μ_L	Dynamic viscosity, of liquid phase
k	turbulent kinetic energy, or number of phases	μ_t	Turbulent viscosity
k_L	Oxygen transfer coefficient	ν	Kinematic viscosity
k_La	Specific oxygen mass transfer coefficient	ζ	Random number
l_e	Kolmogorov length scale	ρ_L	Density of liquid phase
M	Torque	τ_{nn}, τ_{nt}	Stress tensor, nn normal stress, nt shear stress
M_G	Molar mass of gas phase	$\overline{\overline{\tau}}$	Reynolds stress tensor
$\dot{n}$	Molar flux	Mathematic symbols and indices	
N	Rotational speed	G	Gaseous phase
P	Power	L	Liquid phase
p	Pressure	x, y, z	Direction in Cartesian coordinates
P/V	Specific power input	∇	Nabla operator
P_0, Ne	Power number, Newton number	δ	Partial derivative
q_{O2}	Specific oxygen requirement (of cells)	π	Pi
Re	Reynolds number	$\propto$	Proportional
R_k	Term for interphase momentum transport		

dynamics (CFD) modeling has become a widely accepted numerical technique for studying local characteristics (e.g., liquid velocity, gas holdup and shear stress) within both simple and very complex flows [4,5]. In addition, process critical fluid flow parameters, which are hard or even impossible to measure, can be predicted by CFD [6]. Although, experimental methods, such as laser Doppler anemometry (LDA) or particle image velocimetry (PIV), are reliable and required for validation of simulation results, these techniques are too time consuming for the complete characterization of flows in bioreactors [7]. Furthermore, optical accessibility can be a problem, especially for large-scale bioreactors of up to 20 m^3 that are used in biophar-

maceutical production processes [1]. In addition, CFD can provide insights into the fluid flow in single-use bioreactors, which have been increasingly introduced into biotechnological applications during the last two decades. These bioreactors, which are made of rigid or flexible plastic materials, differ from their traditional counterparts in terms of their working principles, mixing and power input. Besides stirred bioreactors, which closely mimic standard bioreactors, wave-mixed and orbitally shaken bioreactors are also used in industry.

In the following the most important engineering parameters for bioreactors, particularly those used for cultivation of suspension cultures, and their influence on the biological systems are introduced. Subsequently, the theoretical basis for CFD and the models that it relies upon are outlined. Recent application examples are then provided, with a special focus on CFD studies for the most frequently used bioreactor types, and on that basis, the potential and the limitations of CFD are discussed. Finally, current trends in the use of CFD for engineering characterization of bioreactors are summarized.

Key Terms

Bioreactor: Device or system in which biochemical reactions take place, catalyzed by organisms or biochemically active substances.

Shear stress: Force acting on fluid elements and suspended particles due to relative motion.

Oxygen mass transfer coefficient: Measure of the ability of a (bio)reactor system to transfer oxygen from the gaseous to the liquid phase.

Computational fluid dynamics: Branch of fluid mechanics to predict fluid flows based on numerically solved models.

Engineering characterization: Estimation and description of characteristic behavior of apparatuses or facilities at specific operating conditions.

Classical & advanced parameters for characterizing bioreactors

One of the most important engineering parameters of bioreactors is the (volume specific) power input P/V, which describes the amount of power that is dissipated within the system and is often related to mechanical strain acting on cells [8,9]. In stirred bioreactors, the power input is directly related to the stirrer torque as given by **Equation 1**, where M, N and V denote the torque acting on the stirrer shaft, the impeller speed and the liquid volume respectively. **Table 1** defines the symbols used throughout the article.

$$\frac{P}{V} = \frac{2\pi \cdot N \cdot M}{V}$$

Equation 1

From P/V the dimensionless power number P_0 (also referred to as Newton number Ne) can be obtained **(Equation 2)**, which is a dimensionless measure of the hydraulic forces acting at the stirrer with the diameter d. It is often used for comparison of different impellers. If a critical level of turbulence is exceeded, the power number becomes constant for many industrially relevant stirrers (e.g., Rushton turbine, pitched blade impeller, marine impeller and so forth).

$$Ne = \frac{P}{\rho_L \cdot N^3 \cdot d^5}$$

Equation 2

The turbulence can be characterized by the dimensionless Reynolds number (Re), which is a measure of the ratio of inertial to viscous forces. For stirred bioreactors, the Reynolds number is defined by **Equation 3**, where ρ_L and μ_L represent the liquid density and dynamic viscosity, respectively. The critical Reynolds number, above which fully turbulent conditions are achieved with most stirrers, is in the order of 1×10^4 to 5×10^4 [10].

$$Re = \frac{\rho_L \cdot N \cdot d^2}{\mu_L}$$

Equation 3

Convection in general, and turbulence in particular, is the driving force for mixing and mass transfer. The ability of a bioreactor to efficiently mix the vessel contents is usually defined by the mixing time t_m, which represents the time required to achieve a desired degree of homogeneity (usually 95%) [11], since it is not possible to achieve a completely homogenous mixture in real-life systems. For stirred reactors under turbulent conditions the following empirical correlation has been established [12]:

$$t_m \propto \frac{P}{V^{-1/3}}$$

Equation 4

Another very important process parameter is the oxygen mass transfer, because most production organisms are growing in aerobic conditions and oxygen has a low solubility in water-like media, which necessitates a continuous aeration of the cultures. Although cell cultures have much lower oxygen requirements than microorganisms, oxygen mass transfer can become the most pronounced process limiting factor in high cell density cultivations or where rigorous sparging/aeration is undesired because of culture shear sensitivity. Nevertheless, the oxygen mass transfer rate (OTR) should be equal to or higher than the oxygen uptake rate (OUR) to prevent the culture from experiencing oxygen depletion. While

the oxygen uptake depends on the specific requirement of the culture (q_{O2}) and the cell concentration (X), the OTR is directly proportional to the mass transfer coefficient (k_La) and the concentration difference between the gas–liquid interface and the bulk fluid (dO_2^*-dO_2), which represents the driving force of the mass transfer.

$$\underbrace{q_{O2} \cdot X}_{OUR} \leq \underbrace{k_L a \cdot (dO_2^* - dO_2)}_{OTR}$$

Equation 5

In CFD studies, the k_La value is commonly derived from the product of the specific surface area 'a', defined by:

$$a = \frac{A_G}{V} = \frac{6 \cdot \alpha_G}{(1 - \alpha_G) \cdot d_B}$$

Equation 6

where A_G represents the surface of the gas phase and V the liquid volume, α_G is the phase fraction of the gaseous phase and d_B is the mean diameter of the gas bubbles, and the mass transfer coefficient k_L. This can be estimated based on Higbie's penetration theory using:

$$k_L = C_1 \cdot \sqrt{D_L} \cdot \left(\frac{\varepsilon_L}{\nu_L}\right)^{0.25}$$

Equation 7

where ε_L represents the dissipation rate of turbulent kinetic energy per unit mass and ν_L the kinematic viscosity, D_L is the oxygen diffusivity (1.98×10^{-9} m^2 s^{-1} in water at 20°C) and C_1 denotes a constant, which is often set to:

$$\frac{2}{\sqrt{\pi}}$$

(in accordance to Higbie's penetration theory) in stirred bioreactors [13]. This approach describes the contact time of gas bubbles (which is the ratio of bubble diameter and bubble slip velocity) based on an eddy cell model, which assumes that mass transfer is mainly dependent on the motion of small-scale eddies in the dissipation range [14].

Obviously, the oxygen transfer can be enhanced by increasing the driving force (e.g., by use of pure oxygen), increasing the turbulence leading to higher k_L values and/or by enhancing the specific gas–liquid surface area. The latter is significantly influenced by the bubble size, where smaller bubbles lead to larger surface areas. Interestingly, CFD studies revealed that local shear or turbulent forces that occur when bubbles burst at the surface of a liquid may exceed the volumetric stirrer power input by some orders of magnitude. The energy associated with the bursting of a 1–2 mm bubble is in the order of 0.1×10^5 to 1×10^5 kW m^{-3}, which is sufficient to destroy suspended animal cells [15]. The reason for the potential damage caused by the bubble burst may be explained by the receding film at the top of the bubble, which is estimated to retreat at approximately 8 m s^{-1} [1].

However, the mechanisms of cell disruption are not yet fully understood, even though huge efforts have been made by several researchers [15–17]. This can also be explained by the difficulty of determining the forces acting on cells within a complex fluid domain such as a bioreactor and the fact that the relationship between lethal/sub lethal forces on cells and their magnitude and exposure time is still unclear [18,19]. In general two flow features, which may be predicted by CFD, are considered to be related to cell damage: spatial gradients of the fluid velocity and turbulence. The velocity gradients act on the cells as shear and normal stresses. Whereas the shear stresses result from velocity gradients normal to the flow direction while normal stresses act in flow direction. The relative importance of both stresses related to cell damage has been controversially discussed for more than a decade [20–22]. However, CFD provides a reliable method of distinguishing between shear and normal forces based on the stress tensor $\overline{\overline{T}}$, which can be represented by **Equation 8**, when the stresses are related to the velocity gradients in incompressible flow according to Stoke's law.

$$\overline{\overline{T}} = \mu \cdot (\nabla \vec{u} + \nabla \vec{u}^T)$$

Equation 8

Based on a coordinate transformation in the CFD fluid domain, it was proposed to calculate the shear (τ_{nt}) and normal (τ_{nn}) stresses by **Equation 9** and **Equation 10**, respectively [23,24], where $\tilde{u}_i$ are velocities in the local coordinate systems defined by the co-ordinates $\tilde{x}$, $\tilde{y}$ and $\tilde{z}$, which are orientated along the fluid flow direction.

$$\tau_{nn} = \mu \cdot \sqrt{2 \cdot \left(\frac{\delta \tilde{u}_x}{\delta \tilde{x}}\right)^2}$$

Equation 9

$$\tau_{nn} = \mu \cdot \sqrt{\left(\frac{\delta \tilde{u}_x}{\delta \tilde{y}} + \frac{\delta \tilde{u}_y}{\delta \tilde{x}}\right)^2 + \left(\frac{\delta \tilde{u}_x}{\delta \tilde{z}} + \frac{\delta \tilde{u}_z}{\delta \tilde{x}}\right)^2}$$

Equation 10

In addition to the shear stresses, the cell damage related to hydrodynamic stress can be estimated based on turbulence parameters. A popular, but yet unproven, assumption suggests that the biological entity is damaged by eddies of a comparable size. Eddies much smaller than cells possess too little energy to cause damage, and eddies much larger than cells will transport them convectively without causing damage. According to the turbulence energy cascade model, the power input is transported to

smaller scales until it dissipates completely [25]. Assuming local isotropic turbulence, the size of the smallest eddies is defined by the Kolmogorov microscale of turbulence l_e (Equation 11). Although it was stated that turbulence in the impeller jet is anisotropic [26,27], theoretical considerations and experimental evidence have shown that the fine-scale structure of most anisotropic turbulent flows is actually almost isotropic locally [28]. Thus, Kolmogorov's definition of eddy size appears suitable for the complete fluid domain defined by:

$$l_e = \left(\frac{\nu^3}{\varepsilon}\right)^{0.25}$$

Equation 11

where v represents the kinematic viscosity and ε the dissipation rate of turbulent kinetic energy per unit mass. Through the velocity gradients and the turbulent dissipation rate, which are predictable by CFD, two parameters are available, which are related to hydrodynamic stress caused on cells. Thus, it can be stated that using CFD more detailed information, which are spatially and time resolved, can be obtained. However, the reliability of these data depends on the applied models and boundary conditions, which are described more detailed in the following.

Definitions & models

A detailed description of the theoretical background of CFD and the solution algorithms can be found in several excellent text books dealing with the basic principles of fluid dynamics [29–31]. Briefly, CFD is based on conservation equations for mass (see Figure 1), momentum and energy, which represents balances of accumulation, net inflow by convection and diffusion as well as volumetric production within a defined volume (i.e., control volume; CV). To predict the fluid flow in bioreactors, the mass and momentum balance of at least one phase are required. However, the local instantaneous velocities, which are necessary to solve the transport equations, fluctuate significantly as a result of the turbulence that occurs under typical bioreactor operating conditions. The direct numerical simulation (DNS) of those fluctuations would require huge processing capacity and, therefore, is still not applicable for industrially relevant bioreactors beyond liter scale. Therefore, the instantaneous velocities u are substituted by time-averaged velocities $\bar{u}$ and the fluctuation velocity u′, which results in the Reynolds-Averaged Navier-Stokes (RANS) equations (Equation 12) representing the most often used approach for CFD analysis of bioreactors from ml to m^3 scale. Here, p represents the static pressure while $\rho \cdot g$ and S denote the gravitational and additional source terms (e.g., centrifugal and Coriolis forces), respectively.

$$\frac{\delta \rho}{\delta t} + \nabla \cdot (\rho \vec{u}) = 0$$

$$\delta(\rho \vec{u}) + \nabla \cdot (\rho \vec{u}\vec{u}) + \nabla p - \nabla \bar{\bar{\tau}} - \rho \vec{g} + S = 0$$

Equation 12

As a result of the time-averaging, the Reynolds stress tensor $\bar{\bar{\tau}}$ is introduced, which is usually calculated by turbulence models based on the Boussinesq hypothesis (eddy viscosity hypothesis) using Equation 13, where δ_{ii} is the Kronecker symbol.

$$\bar{\bar{\tau}} = -\rho \overline{u_i' u_j'} = \mu_t \left(\frac{\delta \overline{u_i}}{\delta x_j} + \frac{\delta \overline{u_j}}{\delta x_i} \right) - \frac{2}{3} \rho k \delta_{ij}$$

$$\mu_t = \rho C_\mu \frac{k^2}{\varepsilon}$$

Equation 13

The turbulent or eddy viscosity μ_t represents a virtual viscosity resulting from the turbulence. Modern CFD codes employ multiple different two-equation turbulence models (e.g., of the k-ε and the k-ω family) as well as several alternative models, including relatively simple single equation models (e.g., Spalart-Allmaras) and the more sophisticated seven-equation Reynolds stress model. The most often applied turbulence model is the k-ε model, where k and ε describe the turbulent kinetic energy and the turbulent dissipation rate, respectively, for which two new balance equations are required:

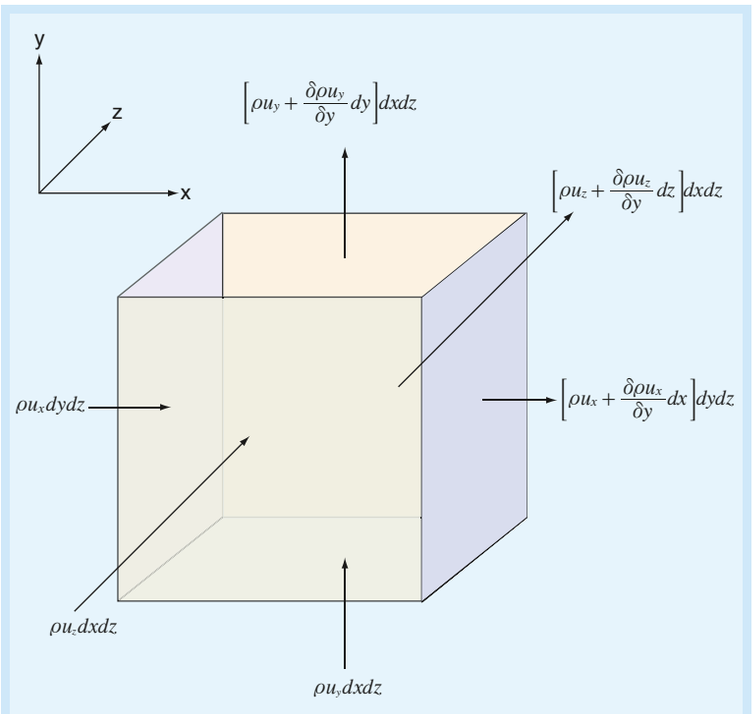

Figure 1. Principle of mass balance at an infinitesimal volume element.

$$\frac{\delta(\rho k)}{\delta t} + \nabla \cdot (\rho k \vec{u}) + \nabla \cdot \left[\left(\mu + \frac{\mu_t}{\sigma_k}\right)\nabla k\right] - G_k - \rho\varepsilon = 0$$
$$\frac{\delta(\rho \varepsilon)}{\delta t} + \nabla \cdot (\rho \varepsilon \vec{u}) + \nabla \cdot \left[\left(\mu + \frac{\mu_t}{\sigma_k}\right)\nabla \varepsilon\right] - C_{1\varepsilon}\frac{\varepsilon}{k}G_k + C_{2\varepsilon} - \rho\frac{\varepsilon^2}{k} = 0$$

Equation 14

where C_1, C_2, C_μ, C_1, σ_k and σ_ε are semi-empirical constants, which are valid for a wide range of flows and G_k represents the generation of turbulence kinetic energy due to the mean velocity gradients. Alternatively to the k-ε turbulence models, the shear-stress transport k-ω model was developed to effectively combine the robust and accurate formulation of the k-ω model in the near-wall region with the free-stream independence of the k-ε model in the far field [32]. Hence, it is preferable for bioreactors with both rough turbulence and (smooth) shear flow, such as rocker-type wave-mixed bioreactors [33]. Thanks to the increasing computing power, the large eddy simulation (LES) approach has been increasingly applied in the last decade [34–37]. Here, large eddies are resolved directly, while small eddies are modeled, which allows much lower spatial and temporal resolution compared with DNS. However, it still requires substantially finer grids than typically used for RANS approaches.

Nevertheless, multiphase flows are mostly found in bioreactors. Besides the aeration typically used for the oxygenation of the aerobic growing production organisms, carrier-based processes (e.g., microcarriers, fluidized beds) can be considered by introduction of a secondary phase [38]. Thus, important engineering parameters, such as gas hold-up, specific surface area and/or oxygen mass transfer rates, can be predicted.

The multiphase model with the least computational effort is represented by the volume-of-fluid (VOF) model, which is based on the assumption that there is no interpenetration between the different phases. Assuming that the phases share the same velocity and pressure field, a single momentum equation is used. To track the interface(s) between the phases, continuity equations for the volume fraction of the phases are introduced. Depending on the phase volume fraction α within the CV, the flow variables and fluid properties are either purely representative of one of the phases, or representative of a mixture of the phases. The density and (molecular) viscosity are calculated by:

$$\rho = \sum \alpha_k \rho_k$$

Equation 15

$$\mu = \sum \alpha_k \mu_k$$

Equation 16

The VOF model is recommended for slug bubbles [39] (or bigger bubbles in general) and free surface flows, as they are found in orbitally shaken (e.g., shake flasks, microtiter plates [40]) or wave-mixed bioreactors [33,41], for example.

In contrast to the VOF model, the Euler–Euler approach (EE; also referred to as the dense phase approach) describes the mass and momentum of each phase separately and, therefore, the interactions between the phases that result in relative motion can be considered. The EE approach is recommended for volume fractions of the dispersed phase that are higher than 10%. The mass and momentum balances are extended by the phase fraction α and can be written for the k^{th} phase as:

$$\delta(\alpha_k \rho_k) + \nabla \cdot (\alpha_k \rho_k \vec{u_k}) = 0$$
$$\frac{\delta(\alpha_k \rho_k \vec{u_k})}{\delta t} + \nabla \cdot (\alpha_k \rho_k \vec{u_k}\vec{u_k}) + \alpha_k \nabla p - \nabla \bar{\bar{\tau}} - \alpha_k \rho_k \vec{g} + S_k - \vec{R_k} = 0$$

Equation 17

where mass transfer between the phases is neglected. The term S_k represents additional source terms and the term $\vec{R_k}$ represents interfacial momentum transport which has been investigated by many researchers [4,42–45]. The most important phase interaction forces are the drag force, the lift force and the virtual mass force, but there is no consensus in literature, whether all forces should be considered in every case. The drag force describes the forces acting on the disperse phase due to relative velocity between the phases, while the lift force is related to velocity gradients of the continuous phase and/or rotation of the disperse phase. Furthermore, the virtual mass force acts on the disperse phase if the dispersed particles accelerate within the surrounding continuous phase. For the numerical details of the required sub-models the interested reader is referred to [4,42–45].

In addition, the Euler–Lagrange approach can be used for multiphase modeling. Here, the description of the continuous (liquid) phase is combined with a segregated description of the dispersed (solid/gas) phase. Based on the flow pattern of the Eulerian phase, the trajectory of the particles of the Lagrangian phase is calculated by **Equation 18**, which inherently requires a time-resolved treatment [31].

$$\frac{d\vec{x}}{dt} = \vec{u}$$

Equation 18

Furthermore, the particles move randomly in turbulent flows as a result of the turbulent dispersion superimposed on the convective flow, which can be estimated by **Equation 19**. Here, $\Delta x_{i,t}$ is the random jump in one dimension (x, y, or z) during a time step of Δt, ζ signifies a random number with a variance of 1,

and D_T stands for the local eddy diffusivity calculated from the continuous phase.

$$\Delta x_{i,t} = \zeta \sqrt{2 D_T \Delta t}$$

Equation 19

The phases are coupled via momentum exchange terms similar to the EE, but the computing effort is much higher due to the separate treatment of each computational particle, which usually still represents a large collective of real particles.

If the disperse phase shows a wide distribution of one or more physical properties, such as size, density or shape, population balances equation (PBE) models can be applied. In bioreactor CFD models, PBE are most often introduced to describe the size distribution of bubbles that occur during aeration, where the bubbles' number density f is included as the characteristic parameter. The number density within a CV can change as a result of convection, bubble coalescence and breakup, gas expansion and mass transfer. This is represented by **Equation 20**, where $\dot{n}$, A_G and M_G denote the molar flux, the bubble surface area and the molar mass of the gas, respectively.

$$\underbrace{\frac{\delta f}{\delta t}}_{\text{Accumulation}} + \underbrace{\nabla \cdot (\vec{u} f)}_{\text{Convection}} + \underbrace{\frac{1}{\rho_G}\frac{d\rho_G}{dt}\frac{\delta (vf)}{\delta v}}_{\text{Gas expansion}} - \underbrace{\frac{\delta}{\delta v}\left(\dot{n} A_G \frac{M_G}{\rho_G} f\right)}_{\text{Mass transfer}} + \underbrace{B_c + D_c - B_b + D_b}_{\text{Bubble break-up and coalescence}} = 0$$

Equation 20

Since both bubble coalescence and break-up lead to a simultaneous increase and decrease in bubble sizes (i.e., two small bubbles merge to one bigger bubble or one big bubble breaks into multiple smaller ones), the PBE includes four source terms that describe the 'birth' (B_c and B_b) and 'death' (D_c and D_b) of bubbles. Calculating these values requires special models, which are mostly derived from turbulence theory. Details of these models are provided elsewhere in the literature [46].

The CFD procedure & verification

The typical steps in the CFD work flow can be subdivided into pre-processing, processing and post-processing (see **Figure 2**). These steps are implemented in the most common CFD codes, such as ANSYS Fluent, ANSYS CFX, FLOWIZARD, PHOENICS, STAR-CCM+ and OpenFOAM.

The first step involves building the geometry model (2D or 3D) and meshing. The above-mentioned CFD packages offer powerful algorithms enabling efficient meshing with 2D (triangle, rectangle, polygons) or 3D (tetrahedrons, hexahedrons, polyhedrons) elements. Nevertheless, compromises often have to be made between fine grids that provide low approximation errors and the increased computational effort required as the number of individual CVs increases (see **Figure 3**). In general, the accuracy increases as the grid is further refined. However, beyond a certain grid density further refinement does not result in any further gains in accuracy. It should be noted that the calculation time increases exponentially as the grid density increases, however this can be reduced by parallelization. The gain in calculation speed by parallelization is, however, not linear as a result of an increase of administrative losses. Besides the applied turbulence models, the discretization of transport phenomena to a finite-spaced grid is considered to be the major reason for the inaccuracy of the numerical solution. Therefore, prior to performing design studies that consider various geometries and/or operating conditions, it is strongly recommended that a grid sensitivity study is carried out to evaluate the accuracy of the numerical solution and the calculation time.

After meshing, suitable models, media properties (density, viscosity, surface tension), initial and

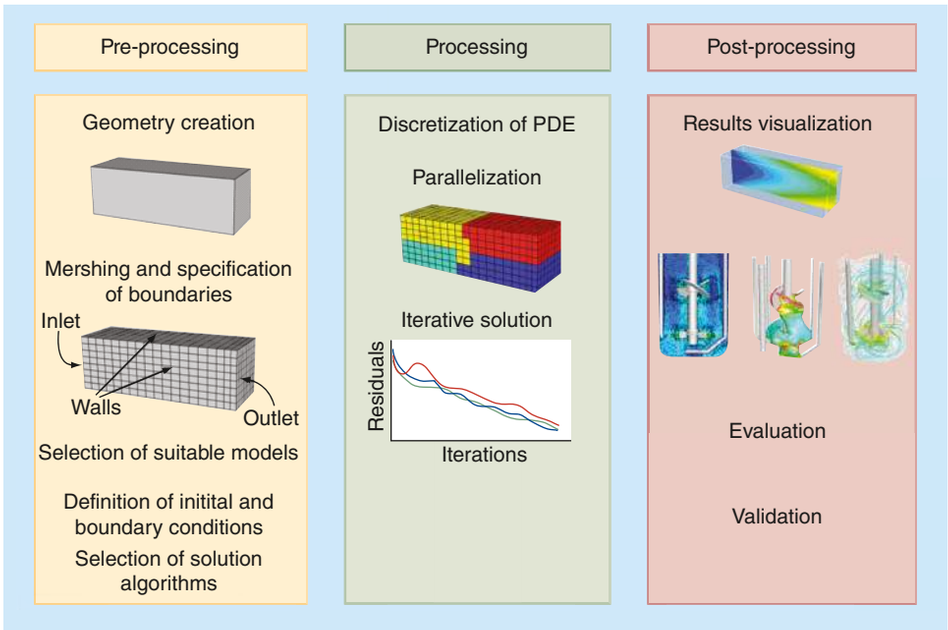

Figure 2. Computational fluid dynamics work flow.
PDE: Partial differential equation.

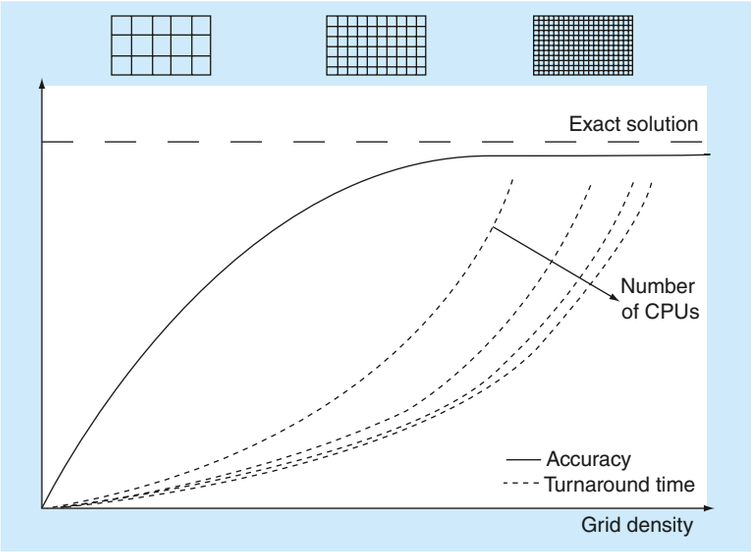

Figure 3. Relationship between accuracy, calculation time and grid density.

boundary conditions (e.g., inlets, outlets, symmetry planes), and solution algorithms have to be defined, depending on the flow of interest. In the next step, which is primarily performed by the CFD software, the partial differential equations are discretized and subsequently solved numerically. To reduce the turnaround time, modern CFD codes can run the process in parallel, which means that several processors are used simultaneously to perform the calculation. Finally, the last step involves interpreting of the data as vectors, contour or path line plots and surface/volume-weighted minimum, mean and maximum values. Since CFD is based on various models and assumptions, the results should be validated by at least some experimental data. For this purpose, several methods have been published, including determination of engineering parameters, such as power input, mixing times, oxygen mass transfer, residence time, or the direct measurement of fluid velocities inside the bioreactor. The latter can be performed by vane or hot-wire anemometers [47], which are in contact with the fluid and may, therefore, influence the flow pattern. Contactless measurement techniques, such as LDA [48], PIV [34], computer-automated radioactive particle tracking [49] or laser-induced fluorescence [50], are preferable. Since the state-of-the-art techniques LDA and PIV, schematically shown in **Figure 4**, use laser systems for the illumination of particles inside the flow, optical accessibility to the vessel content is inherently required.

Application of CFD for characterization of bioreactors

Stirred bioreactors (see **Figure 5A & B**) are the most commonly used bioreactor systems in biotechnological applications. CFD modeling has been performed for the milliliter [51] to cubic meter [52] scale. The stirrer rotation can be integrated in the CFD model using either the dynamic or sliding mesh approach (e.g., as applied by [53,54]). However, the nodes that define the fluid domain must be updated as a function of time and as a result this methodology is inherently unsteady, which requires increased computational power. The multiple reference frame method, where the grid is position-fixed (and thus also referred to 'frozen-rotor'), has been more often applied for both single- [50,55] and multi-phase models [56–59]. In these cases, the flow characteristics of the inner region are used as bound-

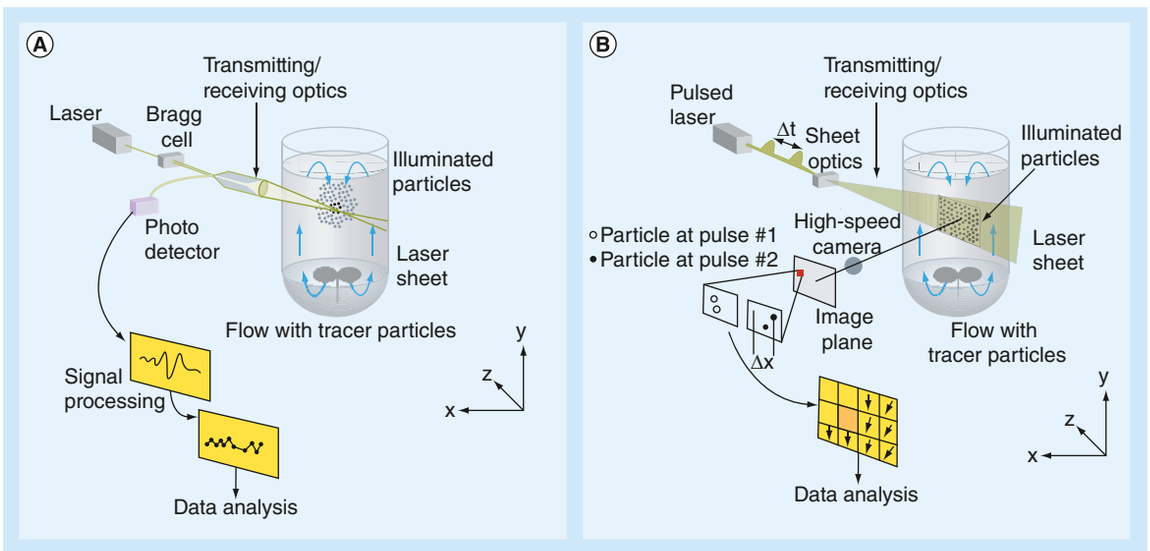

Figure 4. Working principle of measurement techniques. (A) Laser doppler anemometry and **(B)** particle image velocimetry.

ary conditions for the outer region and *vice versa* and a stationary solution is calculated.

After early attempts to characterize the fluid flow patterns of standard stirrers, such as Rushton turbine or pitched blade impellers, in the early 1990s, more specialized impellers found in biotechnological applications have been investigated [60–62]. Szalai *et al.* [60] investigated the mixing performance of four Ekato Intermig® impellers in a laminar flow regime and were able to show that rigorous compartmentalization exists in the vessel as a result of weak axial transport. This may lead to concentration gradients during fermentation processes, but it was found that the build-up of compartments can be suppressed by decreasing the distance between the two lower impellers. Furthermore, a wider range of operating conditions can be made possible by positioning multiple Intermig impellers on a single shaft at 45° angles to each other instead of 90°, as recommended by manufacturers [62].

Besides the classical bioreactors made of glass or stainless steel, the fluid flows in small [63], bench top [64] and pilot scale [33] single-use stirred bioreactors have also been investigated. By comparing wavy-walled spinner flasks with a cylindrical configuration used for tissue engineering applications, Bilgen and Barabino [63] demonstrated that wavy walls reduce the tangential velocity and the maximum shear stress by half in comparison to a cylindrical vessel at identical impeller speeds. This is expected to influence the mechanical properties of cultured tissues. For the unbaffled benchtop scale Mobius® CellReady bioreactor (distributed by Merck Millipore) it was found that the marine impeller induced no clear axial flow profile as expected. However, a dominance of the impeller's radial component with slightly upwards directed impeller discharge was revealed for clockwise rotation only, where the radial discharge of the impeller re-circulated in two axial flow loops from the top and the bottom to the stirrer in each half of the vessel. Small dead zones were identified in the drain port inlet, where cell sedimentation and agglomeration occurred during cultivation of CHO suspension cells [65].

In comparison studies of the single-use benchtop UniVessel® 2L SU bioreactor with a conventional counterpart made of glass, it was discovered that the fluid flow in single-use bioreactors is identical to conventional vessels, provided the geometry of the cultivation container and the impellers is almost identical [41]. However, in several single-use stirred bioreactors, such as the S.U.B. (also known as HyClone™) from ThermoFisher or the Mobius® CellReady 250 from Merck Millipore, the impellers significantly differ from standard configurations. While the first utilizes a three-bladed pitched blade impeller mounted on an eccentric, tilted shaft, the latter is agitated by a bottom-mounted pitched-blade impeller. Hence, complex fluid flow patterns are likely to occur, making detailed flow analysis important. In the case of the HyClone bioreactor, three flow loops were predicted near the bottom indicating well-mixed conditions. However, weak flow was found near the liquid surface when working at maximum filling height [33]. This may lead to inhomogeneities within the vessel contents, especially if media are added at the liquid surface.

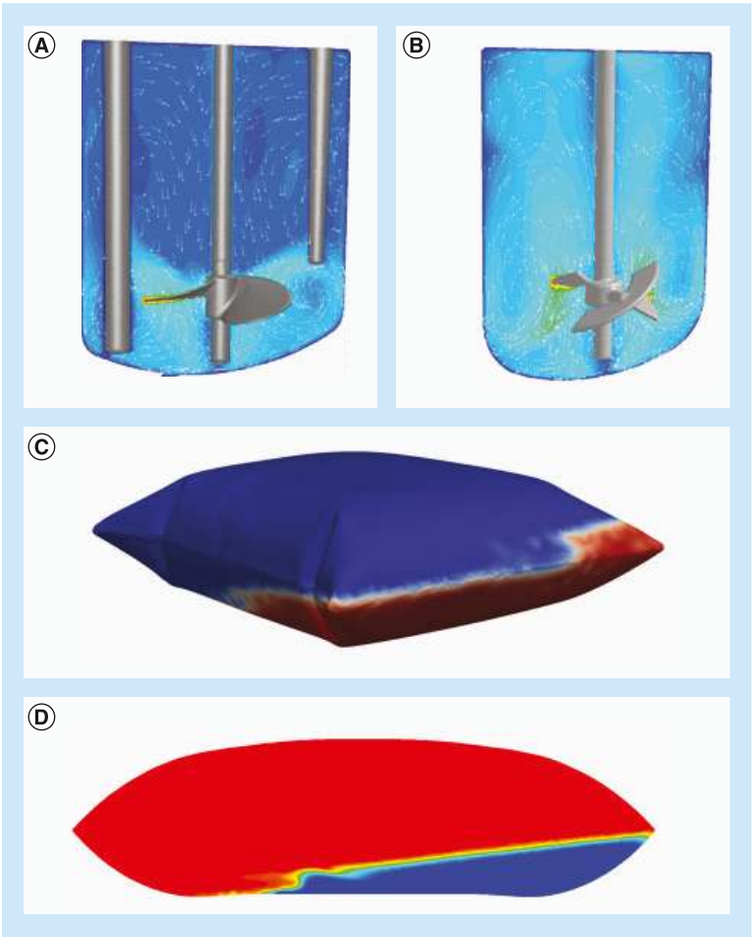

Figure 5. Overview of the most often used bioreactor types for cell culture. (A) Stirred Bioreactor, Mobius® CellReady 3L bioreactor, **(B)** stirred bioreactor, Sartorius Stedim Biotech BIOSTAT® Bplus, **(C)** orbitally shaken bag and **(D)** wave-mixed bioreactor.

The power input in stirred bioreactors is most often predicted through the torque acting on the stirrer (see **Equation 1)** [33,41] and agrees well with experimental data **(Table 2)**. Alternatively, the summation of the (viscous and/or turbulent) energy dissipation rate has been proposed (see **Equation 21**). However, the power input is often significantly under predicted when using this

Table 2. Summary of computational fluid dynamics-predicted and experimentally obtained power numbers of different stirred systems.

Bioreactor/impeller	CFD-predicted power number Ne_{CFD} (-)	Measured power number Ne_{Exp} (-)	Ref.
Retreat curve impeller	1.07	1.02	[94]
Eight-blade paddle impeller	6.6	5.9	[95]
Pitched blade turbine	1.83	1.93	[96]
Miniature parallel bioreactor with RT†	3.7	3.5	[97,98]
Mobius® CellReady 3L	0.33	0.30	[64]
Lightnin A200‡	1.55	1.45	[55]
Double Rushton turbine	8.77	8.46	[59]
SCABA 6SRGT Impeller‡	1.8	1.9	[99]
BIOSTAT® CultiBag STR			[38]
RT and SBI§	3.14	3.4	
SBI and SBI¶	1.13	1.2	

†Comparison of measured power input with CFD data of a cited reference.
‡Value of fully turbulent conditions in shear-thinning solution.
§Combination of RT and SBI.
¶Combination of two SBI.
CFD: Computational fluid dynamics; RT: Rushton turbine; SBI: Segment blade impellers.

method [66]. This may be explained by the use of grids squares that were too large or unsuitable turbulence models, such as the k-ε turbulence model, which does not take into account the anisotropic nature of the turbulence near the impellers [67].

$$\bar{\varepsilon} = \frac{\int \rho \varepsilon dV}{V}$$

Equation 21

Although the occurrence of inhomogeneities is well-known for large-scale bioreactors, mixing can also be challenging for stirrers in ml-scale bioreactors, where fully established turbulence is hard to achieve. The fluid flow in 30 ml stirred minibioreactor was studied by Bulnes-Abundis [50]. The authors found that chaotic flow fields, which, rather than turbulence, are the driving force behind mixing, are pronounced by the use of eccentric stirrers. At the same time segregated or low-rate mixing regions are prevented using round-shaped bottoms. Furthermore, it was demonstrated that the shear stress distribution of the eccentric impeller was narrower and contained a significantly lower frequency of high shear stress values, even at the same Re value as to a conventional Rushton turbine [50]. Compared to the aforementioned parameters, the prediction of residence time distribution and circulation time is of minor importance for the engineering characterization of stirred bioreactors. However, the results of some experiments have been published [68].

In contrast, great attention has been given to (oxygen) gas–liquid mass transfer, which explains the multitude of publications that are concerned with CFD modeling of aerated stirred bioreactors [64,69,70]. Previous studies used single bubble sizes to study gas dispersion in stirred tanks, rather than considering the effects of bubble breakup and coalescence, whereas more recent studies most often include bubble size distributions in their work [56,71,72]. Ahmed *et al.* were among the first to investigate gas–liquid flows in the different flow regimes that prevail in stirred reactors [57]. Their two-fluid CFD model that included the MUSIG model for polydispersed gas has successfully simulated the flow regimes as observed during experiments, enabling the prediction of important flow characteristics, such as gas hold-up, mixing time, and (aerated) power input, over a wide range of operating conditions. Recently, Gelves *et al.* optimized the agitation of a multi-stage impeller in a mammalian cell culture vessel and proposed a stirring and aeration device composed of three pitched blades and three rotating microspargers [73]. Using of this novel agitation method, the CFD-predicted power input was halved while the k_La value, which was determined both numerically and experimentally in very good agreement, was increased 34-fold due to the smaller gas bubbles and more homogenous gas dispersion.

In recent years, chemical reaction kinetics have been increasingly integrated into CFD simulations to investigate the influence of mixing on productivity [58,74]. Ding *et al.* discussed a CFD model for continuous stirred tank reactors for hydrogen production with the aim of optimizing impeller geometry [58]. It was demonstrated that the optimized impeller was able to improve mixing in the reactor at lower impeller speed, meaning higher average hydrogen yield and less start-up time were required. By coupling rates of cell growth, substrate and oxygen consumption to the Navier–Stokes equations, Elqotbi *et al.* showed that, even in just a 5 l laboratory-scale fermenter, local glucose concentrations varied by a factor of two [74]. This is rather unexpected, since mixing times are in the order of seconds compared with fermentation time of several hours. However, it reveals the advantages of spatial resolution of CFD models.

Besides the mechanically driven bioreactors, pneumatically driven airlift and bubble column bioreactors are frequently used. They are characterized by an easy construction due to the lack of any moving parts. Nevertheless, very complex, highly transient flow structures occur in these bioreactors because of the intense liquid circulation, wide bubble size distributions and fluctuating gas hold-up profile. Only a few publica-

tions using the Euler–Lagrange approach appear in literature [75–77]. More often Euler–Euler models are applied [78–81]. Recently, Ghadge *et al.* investigated the dynamic environment within a bubble column used for enzyme catalyzed reactions to evaluate lipase deactivation resulting from the hydrodynamics [78]. Not entirely surprisingly, the specific power input as well as the maximum turbulence dissipation rate, shear stress and normal stress were all found to increase as superficial gas velocities increases. However, none of the flow parameters alone were responsible for the lipase deactivation.

Luo *et al.* investigated the hydrodynamics in a photo airlift bioreactor to predict typical trajectories of phototrophic microorganisms within the bioreactor [81]. Since light intensity always reduces exponentially from the wall to the reactor center, following the Lambert–Beer law, hydrodynamics inside photobioreactors need to be optimized to expose the cells to the light for as long as possible. The turbulent dissipation rate (in the downcomer) was identified as a key hydrodynamic parameter. Therefore, CFD provides a theoretical basis for optimization of the inner structure of photobioreactors, since it can more thoroughly explain the effects of their inner structure on cell growth, which was also determined experimentally [80]. Nevertheless, most CFD models of two-phase flows involve semi-empirical parameters, which have to be adopted to match experimental observations. Further work is needed to reduce the empiricism in the estimation procedures, so as to make it possible to model the complete flow pattern in real bubble column reactors over a wide range of operating conditions using CFD [79].

In R&D, orbitally shaken systems (see **Figure 5C**) such as the shake flasks are one of the most widely used bioreactors [82,83]. CFD has been used to determine oxygen mass transfer and energy dissipation in unbaffled 250-ml shake flasks with typical operating parameters (100–300 rpm, 20–60 mm amplitude, 25–100 ml filling volume). The specific surface is larger than in compared stirred bioreactors by a factor of three, however, k_La is tenfold smaller. This can be explained by a much lower energy dissipation and resulting lower turbulence intensity, which has an influence on oxygen mass transfer [84,85]. Design studies of a newly developed frusto-conical shaking bioreactor revealed a 3% greater specific surface area (which was validated experimentally determined higher oxygen mass transfer) and a 21% lower shear strain compared with a flat bottom shaking bioreactor under the same conditions [86]. This shows the potential of CFD even for classical bioreactors such as shake flasks. The CFD models for the orbitally shaken devices agreed well with experimental measurements using a laser-based flow field visualization [82], and thus CFD can be used as a reliable tool for development and optimization. Similar results for experimentally [85] and CFD [40] characterized microwell plates confirm previously described findings of homogeneous energy dissipation. The maximum local energy dissipation rate of 2 kW m^{-3} was found to be half that of rates that have been shown to cause cell damage [87,88].Furthermore, the volume-averaged energy dissipation rate is regarded as suitable engineering parameter for comparison with other orbitally shaken systems, as long as sufficient oxygen supply is guaranteed. Thus, the cell growth and antibody titer of a IgG1 producing hybridoma cell line were found to be similar in 24-well microtiter plates and 250 ml shake flasks, if comparable distributions of turbulent kinetic energy and dissipation rate occur [40]. The approach is still under investigation, but first results of cultivations with insect and plant cells seem to confirm this approach [89].

Similar to the orbitally shaken systems, reduced shear related cell damage due to homogeneous energy dissipation along with low foaming was expected in rocker-type wave mixed bioreactors (see **Figure 5D**) [90]. This was confirmed by time-resolved 3D CFD studies using the VOF model considering various rocking rates and rocking angles at different filling levels up to 20 l, which correctly describe the free fluid surface as observed in video sequences [91]. The obtained shear stress levels, which were verified by hot-film probe measurements, are well below known threshold values that lead to damage of animal cells [92]. Furthermore, the distribution of the energy dissipation is more homogenous in comparison to other bioreactors (e.g., stirred or vibrating disk), meaning they are suitable cultivating shear sensitive biological entities [33].

Conclusion & future perspective

It can be stated that the prediction of general mean flow quantities in single-phase systems can be expected to be valid, even if less sophisticated RANS methods are used. However, the prediction of turbulence parameter and related phenomena is much less accurate. In particular, the grid dependency of certain flow parameters related to cell damage/death (e.g., shear stress and turbulence intensity) still remains an open question. Although predictions by RANS simulations are realistic and can mostly be performed using affordable computer memory with acceptable computational times, the results are strictly dependent on the turbulent model used for the closure problem (i.e., estimation of the six

unknown components of the Reynolds stress tensor). Therefore, numerical uncertainties should be verified carefully.

While previously classical RANS simulations were exclusively used for flow predictions (and still dominate this area), more sophisticated LES simulations have increasingly been introduced during the last decade [34–36,93]. Recently, Liovic *et al.* found excellent agreement between CFD-predicted and experimentally measured velocities in small-scale stirred spinner flasks used for microcarrier based cultivations [53]. Even earlier, Kulkarni *et al.* showed that through the use of the LES turbulence model, mean axial velocities and gas hold-up in a bubble column reactor could be well-predicted [79]. Nowadays, the tremendous computational cost for multiphase flows, for example, approximately 30 days of CPU time for a typical job [37], makes LES still unacceptable in engineering applications. Nevertheless, as computing power further increases, even the highly expensive DNS techniques may become attractive in the future.

The latest developments in using CFD for the characterization of bioreactors and their optimization involve the coupling of complex hydrodynamics of (multiphase) flows with reaction kinetics. It has been shown by several researchers, that fluid flow predictions can be improved when bubble size distributions are taken into account, which are most often calculated using population balance models. Although bubble coalescence is often suppressed in cell culture media because of salt concentrations and the addition of antifoam, it may be essential to consider bubble coalescence and breakage phenomena, since these mechanisms may be responsible for the formation of poorly oxygenated zones.

In the future, investigations considering fluid–structure interactions may become attractive. This is especially the case in single-use bioreactors consisting of flexible bags, where the shapes of the cultivation bags can be influenced by the liquid motion. Furthermore, the shaft of stirred single-use bioreactors is not as tightly fixed as in their conventional counterparts, which may have an influence on the fluid flow patterns. However, no studies into these issues have yet been published.

Financial & competing interests disclosure

The authors have no relevant affiliations or financial involvement with any organization or entity with a financial interest in or financial conflict with the subject matter or materials discussed in the manuscript. This includes employment, consultancies, honoraria, stock ownership or options, expert testimony, grants or patents received or pending, or royalties.

No writing assistance was utilized in the production of this manuscript.

Executive summary

Bioreactor characterization

- The spatial and temporal resolution of the results achieved using computational fluid dynamics (CFD) increase our knowledge of the fluid mechanics within bioreactors.
- Process crucial factors may be recognized early in the development process and may reduce the need for prototyping and shorten the time-to-market.

CFD & its verification

- The numerical solution of the transport equations is realized by means of spatial and temporal discretization of the fluid domain and modeling of turbulence phenomena.
- An experimental verification of simulations results with sophisticated methods, such as particle image velocimetry or laser doppler anemometry, is advisable.

Application of CFD in bioreactor characterization

- The results of a CFD simulation include, amongst others, the velocity in all spatial directions, as well as information about pressure and turbulence.
- The results and their derivatives can be used to develop and optimize bioreactors in order to, for example, avoid inhomogeneities, reduce shear strain (particularly for sensitive cells) and/or increase (gas) mass transfer.

Future perspective

- Direct numerical simulations and/or large eddy simulations can, to a great extent or even completely, remove the need to model turbulence, which may increase accuracy and reliability.
- Sophisticated multiphase models (including population balance models) with additional coupling of chemical reactions may further increase process understanding.
- Single-use bioreactor development and optimization may benefit from models which describe the interaction of fluid and structural mechanics in order to simulate the fluid flow and the associated deformation of bag bioreactors.

References

1 Nienow AW. Reactor engineering in large scale animal cell culture. *Cytotechnology* 50, 9–33 (2006).

2 Eibl R, Eibl D. Disposable bioreactors for inoculum production and protein expression. In: *Animal Cell Biotechnology: Methods and Protocols.* Pörtner R (Ed.). Humana Press, Totowa, NJ, USA, 321–335 (2007).

3 Paschedag AR, Kassera V, Sperling R. Aktuelle entwicklungen in der CFD für gerührte systeme. *Chem. Ing. Tech.* 79, 983–999 (2007).

4 Kelly WJ. Using computational fluid dynamics to characterize and improve bioreactor performance. *Biotechnol. Appl. Biochem.* 49, 225–238 (2008).

5 Fang Z. Applying computational fluid dynamics technology in bioprocesses. *BioPharm Int.* 23, 38 (2010).

6 Sharma C, Malhotra D, Rathore AS. Review of computational fluid dynamics applications in biotechnology processes. *Biotechnol. Prog.* 27, 1497–1510 (2011).

7 Hutmacher DW, Singh H. Computational fluid dynamics for improved bioreactor design and 3D culture. *Trends Biotechnol.* 26, 166–172 (2008).

8 Eibl R, Werner S, Eibl D. Disposable bioreactors for plant liquid cultures at litre-scale. *Eng. Life Sci.* 9, 156–164 (2009).

9 Werner S, Eibl R, Lettenbauer C *et al.* Innovative, non-stirred bioreactors in scales from milliliters up to 1000 liters for suspension cultures of cells using disposable bags and containers – a swiss contribution. *Chim. Int. J. Chem.* 64, 819–823 (2010).

10 Liepe F, Sperling R, Jembere S. *Rührwerke – Theoretische Grundlagen, Auslegung Und Bewertung.* Eigenverlag FH, Anhalt, Köthen, Germany (1998).

11 Werner S, Kraume M, Eibl D. Bag mixing systems for single-use. In: S*ingle-use technology in biopharmaceutical manufacture.* Eibl R, Eibl D (Eds). John Wiley and Sons, Inc., Hoboken, NJ, USA (2011).

12 Löffelholz C, Kaiser, SC. Kraume M, Eibl R, Eibl D. Dynamic single-use bioreactors used in modern liter- and m(3)- scale biotechnological processes: engineering characteristics and scaling up. *Adv. Biochem. Eng. Biotechnol.* 138, 1–44 (2013).

13 Alves SS, Vasconcelos JMT, Orvalho SP. Mass transfer to clean bubbles at low turbulent energy dissipation. *Chem. Eng. Sci.* 61, 1334–1337 (2006).

14 Lamont JC, Scott DS. An eddy cell model of mass transfer into the surface of a turbulent liquid. *AIChE J.* 16, 513–519 (1970).

15 Ma NN, Koelling KW, Chalmers JJ. Fabrication and use of a transient contractional flow device to quantify the sensitivity of mammalian and insect cells to hydrodynamic forces. *Biotechnol. Bioeng.* 80, 428–437 (2002).

16 Thomas CR, al Rubeai M, Zhang Z. Prediction of mechanical damage to animal cells in turbulence. *Cytotechnology* 15, 329–335 (1994).

17 Wurm M, Zeng AP. Mechanical disruption of mammalian cells in a microfluidic system and its numerical analysis based on computational fluid dynamics. *Lab Chip* 12, 1071–1077 (2012).

18 Gregoriades N, Clay J, Ma N, Koelling K, Chalmers JJ. Cell damage of microcarrier cultures as a function of local energy dissipation created by a rapid extensional flow. *Biotechnol. Bioeng.* 69, 171–182 (2000).

19 Mollet M, Ma N, Zhao Y, Brodkey R, Taticek R, Chalmers JJ. Bioprocess equipment: characterization of energy dissipation rate and its potential to damage cells. *Biotechnol. Prog.* 20, 1437–1448 (2004).

20 Langer G, Deppe A. Zum verständnis der hydrodynamischen beanspruchung von partikeln in turbulenten rührerströmungen. *Chem. Ing. Tech.* 72, 31–41 (2000).

21 Wollny S, Sperling R, Kraume M, Ritter J. Beanspruchung von partikeln und fluidelementen beim rühren. *Chem. Ing. Tech.* 79 (7), 1024–1028 (2007).

22 Chisti Y. Hydrodynamic damage to animal cells. *Crit. Rev. Biotechnol.* 21, 67–110 (2001).

23 Wollny S. *Experimentelle und numerische Untersuchungen zur Partikelbeanspruchung in gerührten (Bio-)Reaktoren.* Dissertation, Technische Universität Berlin, Germany (2010).

24 Krause B. *Strömungsabhängige Darstellung der Geschwindigkeitsgradienten. 10. Köthener Rührerkolloquium*. Köthen, Germany (2007).

25 Richardson LF. The supply of energy from and to atmospheric eddies. *Proc. R. Soc. London, Ser. A.* 97, 34–373 (1920).

26 Ranade, VV, Joshi, JB. Flow generated by pitched blade turbines I: measurements using laser Doppler anemometer. *Chem. Eng. Commun.* 81, 197–224 (1989).

27 Jaworski Z, Nienow AW, Koutsakos K, Dyster K, Bujalski W. An LDA study of turbulent flow in a baffled vessel agitated by a pitched blade turbine. *Chem. Eng. Res. Des.* 69, 313–320 (1991).

28 Hinze JO. *Turbulence: An Introduction to its Mechanism and Theory*. McGraw-Hill, NY, USA (1959).

29 Wilcox, DC. *Turbulence modeling for CFD*. DCW Industries, La Canada, CA, USA (1994).

30 Ferziger JH, Peric M. *Computational Methods for Fluid Dynamics*. Springer-Verlag, Berlin, Germany (2002).

31 Paschedag AR. *CFD in der Verfahrenstechnik – Allgemeine Grundlagen und mehrphasige Anwendungen.* Wiley-VCH, Weinheim, Germany (2004).

32 Menter FR. Two-equation eddy-viscosity turbulence models for engineering applications. *AIAA J.* 32, 1598–1605 (1994).

33 Löffelholz C, Kaiser SC, Werner S, Eibl D. CFD as tool to characterize single-use bioreactors. In: *Single-Use Technology in Biopharmaceutical Manufacture.* Eibl R, Eibl D (Eds). John Wiley and Sons, Inc., Hoboken, NJ, USA 263–279 (2011).

34 Delafosse A, Line A, Morchain J, Guiraud P. LES and URANS simulations of hydrodynamics in mixing tank: comparison to PIV experiments. *Chem. Eng. Res. Des.* 86, 1322–1330 (2008).

35 Murthy BN, Joshi JB. Assessment of standard, RSM and LES turbulence models in a baffled stirred vessel agitated by various impeller designs. *Chem. Eng. Sci.* 63, 5468–5495 (2008).

36 Guha D, Ramachandran PA, Dudukovic MP, Derksen JJ. Evaluation of large Eddy simulation and Euler-Euler CFD

models for solids flow dynamics in a stirred tank reactor. *AIChE J.* 54, 766–778 (2008).

37 Zhang Y, Yang C, Mao Z. Large eddy simulation of the gas–liquid flow in a stirred tank. *AIChE J.* 54, 1963–1974 (2008).

38 Kaiser S, Jossen V, Schirmaier C *et al.* Fluid flow and cell proliferation of mesenchymal adipose-derived stem cells in small-scale, stirred, single-use bioreactors. *Chem. Ing. Tech.* 85, 95–102 (2013).

39 Wei P, Zhang K, Gao W, Kong L, Field R. CFD modeling of hydrodynamic characteristics of slug bubble flow in a flat sheet membrane bioreactor. *J. Memb. Sci.* 445, 15–24 (2013).

40 Barrett TA, Wu A, Zhang H, Levy MS, Lye GJ. Microwell engineering characterization for mammalian cell culture process development. *Biotechnol. Bioeng.* 105, 260–275 (2010).

41 Kaiser SC, Löffelholz C, Werner S, Eibl D. CFD for characterizing standard and single-use stirred cell culture bioreactors. In: *Computational Fluid Dynamics Technologies and Applications*. Minin IV, Minin OV (Eds). InTech, Rijeka, Croatia, 97–122 (2011).

42 Joshi JB. Computational flow modelling and design of bubble column reactors. *Chem. Eng. Sci.* 56, 5893–5933 (2001).

43 Massoudi M. Constitutive relations for the interaction force in multicomponent particulate flows. *Int. J. Non. Linear. Mech.* 38, 313–336 (2003).

44 Bhole MR, Joshi JB, Ramkrishna D. CFD simulation of bubble columns incorporating population balance modeling. *Chem. Eng. Sci.* 63, 2267–2282 (2008).

45 Ekambara K, Nandakumar K, Joshi JB. CFD simulation of bubble column reactor using population balance. *Ind. Eng. Chem. Res.* 47, 8505–8516 (2008).

46 Wang T, Wang J, Jin Y. Population balance model for gas–liquid flows: influence of bubble coalescence and breakup models. *Ind. Eng. Chem. Res.* 44, 7540–7549 (2005).

47 Mavros P. Flow visualization in stirred vessels. *Chem. Eng. Res. Des.* 79, 113–127 (2001).

48 Jaworski Z, Nienow AW, Dyster KN. An LDA study of the turbulent flow field in a baffled vessel agitated by an axial, down-pumping hydrofoil impeller. *Can. J. Chem. Eng.* 74, 3–15 (1996).

49 Khopkar AR, Rammohan AR, Ranade VV, Dudukovic MP. Gas–liquid flow generated by a Rushton turbine in stirred vessel: CARPT/CT measurements and CFD simulations. *Chem. Eng. Sci.* 60, 2215–2229 (2005).

50 Bulnes-Abundis D, Carrillo-Cocom LM, Aráiz-Hernández D *et al.* A simple eccentric stirred tank mini-bioreactor: mixing characterization and mammalian cell culture experiments. *Biotechnol. Bioeng.* 110, 1106–1118 (2013).

51 Lamping SR, Zhang H, Allen B, Shamlou PA. Design of a prototype miniature bioreactor for high throughput automated bioprocessing. *Chem. Eng. Sci.* 58, 747–758 (2003).

52 Zou X, Xia JY, Chu J, Zhuang YP, Zhang SL. Real-time fluid dynamics investigation and physiological response for erythromycin fermentation scale-up from 50 L to 132 m(3) fermenter. *Bioprocess Biosyst. Eng.* 35, 789–800 (2012).

53 Liovic P, Šutalo ID, Stewart R, Glattauer V, Meagher L. Fluid flow and stresses on microcarriers in spinner flask bioreactors. Presented at: *Ninth International Conference on CFD in the Minerals and Process Industries CSIRO*. Melbourne, Australia, 10–12 December 2012.

54 Huang W, Li K. CFD simulation of flows in stirred tank reactors through prediction of momentum source. In: *Nuclear Reactor Thermal Hydraulics and Other Application*s. Guillen D (Ed.). InTech, Rijeka, Croatia (2013).

55 Ein-Mozaffari F, Upreti, SR. Investigation of mixing in shear thinning fluids using computational fluid dynamics. In: *Computational Fluid Dynamics*. Oh HW (Ed.). InTech, Rijeka, Croatia (2010).

56 Kerdouss F, Bannari A, Proulx P, Bannari R, Skrga M, Labrecque Y. Two-phase mass transfer coefficient prediction in stirred vessel with a CFD model. *Comput. Chem. Eng.* 32, 1943–1955 (2008).

57 Ahmed SU, Ranganathan P, Pandey A, Sivaraman S. Computational fluid dynamics modeling of gas dispersion in multi impeller bioreactor. *J. Biosci. Bioeng.* 109, 588–597 (2010).

58 Ding J, Wang X, Zhou XF, Ren NQ, Guo WQ. CFD optimization of continuous stirred-tank (CSTR) reactor for biohydrogen production. *Bioresour. Technol.* 101, 7005–7013 (2010).

59 Taghavi M, Zadghaffari R, Moghaddas J, Moghaddas Y. Experimental and CFD investigation of power consumption in a dual Rushton turbine stirred tank. *Chem. Eng. Res. Des.* 89, 280–290 (2011).

60 Szalai ES, Arratia P, Johnson K, Muzzio FJ. Mixing analysis in a tank stirred with Ekato Intermig® impellers. *Chem. Eng. Sci.* 59, 3793–3805 (2004).

61 Mohiuddin AKM, Adeyemi N, Mirghani MES *et al.* Simulation and experimental validation: waste cooking oil transesterification using rushton and elephant ear impellers. Computational intelligence and bioinformatics/755: modelling, identification, and simulation. ACTAPRESS, Calgary, Canada, 228–230 (2011).

62 Aubin J, Xuereb C. Design of multiple impeller stirred tanks for the mixing of highly viscous fluids using CFD. *Chem. Eng. Sci.* 61, 2913–2920 (2006).

63 Bilgen B, Barabino GA. Modeling of bioreactor hydrodynamic environment and its effects on tissue growth. In: *Computer-Aided Tissue Engineering*. Liebschner MAK (Ed.). Humana Press, Totowa, NJ, USA, 237–255 (2012).

64 Kaiser SC, Eibl R, Eibl D. Engineering characteristics of a single-use stirred bioreactor at bench-scale: the Mobius Cell Ready 3L bioreactor as a case study. *Eng. Life Sci.* 11, 359–368 (2011).

65 Eibl R, Kaiser S, Lombriser R, Eibl D. Disposable bioreactors: the current state-of-the-art and recommended applications in biotechnology. *Appl. Microbiol. Biotechnol.* 86, 41–49 (2010).

66 Coroneo M, Montante G, Paglianti A, Magelli F. CFD prediction of fluid flow and mixing in stirred tanks: numerical issues about the RANS simulations. *Comput. Chem. Eng.* 35, 1959–1968 (2011).

67 Lane GL, Koh PTL. CFD Simulation of a rushton turbine in a baffled tank. Presented at: *The proceedings of the third international conference on computational fluid dynamics in mineral and metal processing and power generation*. Clayton, Victoria, Australia, 3–4 July 1997.

68 Zhang L, Pan Q, Rempel GL. Residence time distribution in a multistage agitated contactor with newtonian fluids: CFD prediction and experimental validation. *Ind. Eng. Chem. Res.* 46, 3538–3546 (2007).

69 Moilanen P, Laakkonen M, Aittamaa J. Modeling aerated fermenters with computational fluid dynamics. *Ind. Eng. Chem. Res.* 45, 8656–8663 (2006).

70 Yu P, Lee T, Zeng Y, Low HT. A 3D analysis of oxygen transfer in a low-cost micro-bioreactor for animal celll suspension culture. *Comput. Methods Programs Biomed.* 85, 59–68 (2007).

71 Zhang H, Zhang K, Fan SD. CFD simulation coupled with population balance equations for aerated stirred bioreactors. *Eng. Life Sci.* 9, 421–430 (2009).

72 Martin M, Montes F, Galan MA. Mass transfer rates from bubbles in stirred tanks operating with viscous fluids. *Chem. Eng. Sci.* 65, 3814–3824 (2010).

73 Gelves R, Dietrich A, Takors R. Modeling of gas–liquid mass transfer in a stirred tank bioreactor agitated by a Rushton turbine or a new pitched blade impeller. *Bioprocess Biosyst. Eng.* (2013) (Epub ahead of print).

74 Elqotbi M, Vlaev, SD, Montastruc L, Nikov I. CFD modelling of two-phase stirred bioreaction systems by segregated solution of the Euler–Euler model. *Comput. Chem. Eng.* 48, 113–120 (2013).

75 Laı´n S, Bröder D, Sommerfeld M, Göz MF. Modelling hydrodynamics and turbulence in a bubble column using the Euler–Lagrange procedure. *Int. J. Multiph. Flow.* 28, 1381–1407 (2002).

76 Sokolichin A, Eigenberger G, Lapin A, Lübert A. Dynamic numerical simulation of gas–liquid two-phase flows Euler/Euler versus Euler/Lagrange. *Chem. Eng. Sci.* 52, 611–626 (1997).

77 Delnoij E, Kuipers JAM, van Swaaij WPM. Computational fluid dynamics applied to gas–liquid contactors. *Chem. Eng. Sci.* 52, 3623–3638 (1997).

78 Ghadge, RS, Ekambara K, Joshi, JB. Role of hydrodynamic flow parameters in lipase deactivation in bubble column reactor. *Chem. Eng. Sci.* 60, 6320–6335 (2005).

79 Kulkarni, AA, Ekambara K, Joshi, JB. On the development of flow pattern in a bubble column reactor: experiments and CFD. *Chem. Eng. Sci.* 62, 1049–1072 (2007).

80 Yu G, Li Y, Shen G *et al.* A novel method using CFD to optimize the inner structure parameters of flat photobioreactors. *J. Appl. Phycol.* 21, 719–727 (2009).

81 Luo HP, Al-Dahhan MH. Verification and validation of CFD simulations for local flow dynamics in a draft tube airlift bioreactor. *Chem. Eng. Sci.* 66, 907–923 (2011).

82 Kim HM, Kizito JP. Stirring free surface flows due to horizontal circulatory oscillation of a partially filled container. *Chem. Eng. Commun.* 196, 1300–1321 (2009).

83 Büchs J. Introduction to advantages and problems of shaken cultures. *Biochem. Eng.* J. 7, 91–98 (2001).

84 Zhang H, Williams-Dalson W, Keshavarz-Moore E, Shamlou PA. Computational-fluid-dynamics (CFD) analysis of mixing and gas–liquid mass transfer in shake flasks. *Biotechnol. Appl. Biochem.* 41, 1–8 (2005).

85 Zhang XW, Burki CA, Stettler M *et al.* Efficient oxygen transfer by surface aeration in shaken cylindrical containers for mammalian cell cultivation at volumetric scales up to 1000 L. *Biochem. Eng. J.* 45, 41–47 (2009).

86 Hang HF, Guo YX, Liu J *et al.* Computational fluid dynamics modeling of an inverted frusto-conical shaking bioreactor for mammalian cell suspension culture. *Biotechnol. Bioprocess Eng.* 16, 567–575 (2011).

87 Mollet M, Godoy-Silva R, Berdugo C, Chalmers JJ. Computer simulations of the energy dissipation rate in a fluorescence-activated cell sorter: implications to cells. *Biotechnol. Bioeng.* 100, 260–272 (2008).

88 Godoy-Silva R, Chalmers JJ, Casnocha SA, Bass LA, Ma N. Physiological responses of CHO cells to repetitive hydrodynamic stress. *Biotechnol. Bioeng.* 103, 1103–1117 (2009).

89 Werner S, Olownia J, Egger D, Eibl D. An approach for scale-up of geometrically dissimilar orbitally shaken single-use bioreactors. *Chem. Ing. Tech.* 85, 118–126 (2013).

90 Singh V Disposable bioreactor for cell culture using wave-induced agitation. *Cytotechnology* 30, 149–158 (1999).

91 Eibl R, Werner S, Eibl D. Bag bioreactor based on wave-induced motion: characteristics and applications. *Adv. Biochem. Eng. Biotechnol.* 115, 55–87 (2010).

92 Öncül AA, Kalmbach A, Genzel Y, Reichl U, Thevenin D. Characterization of flow conditions in 2 L and 20 L wave bioreactors (R) using computational fluid dynamics. *Biotechnol. Prog.* 26, 101–110 (2010).

93 Feng X, Cheng J, Li X, Yang C, Mao ZS. Numerical simulation of turbulent flow in a baffled stirred tank with an explicit algebraic stress model. *Chem. Eng. Sci.* 69, 30–44 (2012).

94 Li M, White G, Wilkinson D, Roberts KJ. Scale up study of retreat curve impeller stirred tanks using LDA measurements and CFD simulation. *Chem. Eng. J.* 108, 81–90 (2005).

95 Murthy Shekhar S, Jayanti S. CFD Study of power and mixing time for paddle mixing in unbaffled vessels. *Chem. Eng. Res. Des.* 80, 482–498 (2002).

96 Aubin J, Fletcher D, Xuereb C. Modeling turbulent flow in stirred tanks with CFD: the influence of the modeling approach, turbulence model and numerical scheme. *Exp. Therm. Fluid Sci.* 28, 431–445 (2004).

97 Gill NK, Appleton M, Baganz F, Lye GJ. Quantification of power consumption and oxygen transfer characteristics of a stirred miniature bioreactor for predictive fermentation scale-up. *Biotechnol. Bioeng.* 100, 1144–1155 (2008).

98 Gill NK, Appleton M, Baganz F, Lye GJ. Design and characterization of a miniature stirred bioreactor system for parallel microbial fermentations. *Biochem. Eng. J.* 39, 164–176 (2008).

99 Ameur H, Bouzit M, Helmaoui M. Numerical study of fluid flow and power consumption in a stirred vessel with a Scaba 6SRGT impeller. *Chem. Process Eng.* 32(4), 351–366 (2012).